National Technical University of Athens

SHEAR CAPACITY AND BEHAVIOUR OF REINFORCED CONCRETE STRUCTURAL ELEMENTS WITH DEBONDED REINFORCEMENTS

By

Isaac Michael
Pegah Behinaein

Thesis submitted in partial fulfilment of the requirements for the degree of Master of Science in Civil Engineering; Specialized in Analysis and Design of Earthquake Resistant Structures

School of Civil Engineering
National Technical University of Athens

Supervisor: **Prof. Michael D. Kotsovos**

July, 2013

Declaration

We, Isaac Michael and Pegah Behinaein, declare that the contents of this thesis represent our own work, and that the thesis has not previously been submitted towards any qualification.

Signed **Date**

Signed **Date**

Abstract

Shear failures in concrete structures are very hazardous. These failures can rarely be predicted and often happen explosively. For decades, tests have been done to study this phenomenon, in order to try to understand the shear cracking mechanism in reinforced concrete (RC) beams. Hence, attempts to analytically quantify the mechanism of shear cracking have not been successful to date. However, shear in the current codes are based on empirical procedures.

The initiation of the critical shear cracking is associated with the magnification of actual shear stress produced by a distinct local stress concentration effect arising from the formation of the nearby flexural cracks. This local shear stress concentration is produced by the nature of bond between the concrete and the flexural reinforcements. Thus, it is well established that bond failure at the interface between concrete and flexural reinforcement leads to inclined ("shear") cracking in RC beams.

The main aim of this dissertation is to investigate the possibility of solving the shear problem by preventing the formation, rather than the extension, of inclined cracking in the critical regions of RC beam elements. Since the causes of such cracking are inextricably linked with the interaction between concrete and the longitudinal steel bars, it is attempted to prevent inclined crack formation by preventing concrete-steel interaction through the use of a PVC pipe to cover over the critical region of simply supported beam specimens.

The specimens tested consist of eight rectangular and square reinforced concrete beams, and all the beams have the same length and longitudinal reinforcement. All beams were simply supported and tested under symmetrical two-point loads at mid span. Six of the eight specimens were subjected to sequential loading comprising axial (N) and transverse (P) components, and the rest to a transverse loading only. For two of the beams, external transverse reinforcement was designed in the shear span.

The results obtained indicate that with the use of a PVC cover to the portion of the flexural bars within the critical regions of the beam elements, shear cracking is prevented in all the beams investigated. All the beam specimens failed because of

flexural cracks formed in the mid span. The initiation of this flexural cracking is found to be produced by the nature of bond between the concrete and the portion of the exposed flexural reinforcement. Designing transverse reinforcement for two of the test beams is effective to face the tensile force formed in the interface of cracked and uncracked concrete in the shear span. It is realized that the steel bars in all the beams did not yield and failure happened in concrete only. For further investigation, it is recommended to check the design of longitudinal reinforcements of the beam as it was designed based on full concrete-steel interaction. Thus, this new concept of the bond-prevented flexural failure may lead to savings of the amount of steel bars.

Acknowledgments

We are grateful to our Professor Michael D. Kotsovos for his supervision for entire research and his apparently inexhaustible energy was our primary source of inspiration for completing the research.

We also wish to acknowledge Professor Manolis Papadrakakis, Director of the MSc ADERS Programme, School of Civil Engineering, NTUA for his helps, support, and continuous encouragement during study of Master Program.

We like to thank the Staff of Concrete Laboratory for their cooperation during the experimental work.

As final, we would like to thank Dr. Setayesh Behinaein for his consistent help for revising the research.

Dedication

We would like to dedicate this research to:
Our fathers and mothers who shows us love, patience, responsibilities and hard working
Brothers, sisters, relatives and friends; for their supports to us during hard time.
Teachers and colleagues; for their love and affection to us.
Lastly but not the least to the National Technical University of Athens, School of Civil Engineering.

Table of Contents

List of Figures

List of Tables

List of Symbols and Abbreviations

a_v	Shear span
b	Width of cross section
d	Effective depth of cross section
h	Height of cross section
x	Thickness of compressive part
z	Internal lever arm
f_c	Uniaxial cylinder compressive strength of concrete
f_y	Yield stress of steel bar
f_s	Stress of steel bar
M_f	Flexural capacity
M_y	Bending moment at first yield assumed to occur when either the concrete strain at the extreme compressive fibre attains a value of 0.0035 or the tension reinforcement yields
N_u	Maximum axial force sustained by the specimen under concentric compression
N	Axial force
P	Transverse force
P_{exp}	Experimentally-established load-carrying capacity
M_{exp}	Bending moment corresponding to $Pexp$
P_f	Load-carrying capacity of beam corresponding to M_f
V_f	Half value of P_f
RC	Reinforced Concrete
CFP	Compressive Force Path

Chapter 1: Introduction

This research involves experimental investigation of beams with de-bonded longitudinal reinforcement in order to increase their shear capacity. The bond is removed to prevent the formation of local stress concentration which leads to shear crack.

Behaviour of 8 reinforced concrete beam specimens is investigated. Two of the beams are subjected to monotonic loading and the other 6 are subjected to monotonic loading combined with a constant axial force. The specimens are divided into two categories of square and rectangular cross-sections with same lengths. The beams are de-bonded over the shear span of the beam. Five beams have longer de-bonded reinforcement compared to the rest of the beams.

The results from previous experiments show that the initiation of flexural shear cracking was strongly associated with the bond between concrete and reinforcement. When the application of this method is combined with de-bonding the longitudinal reinforcement, a significant improvement in structural behaviour is achieved [7].

Chapter 2: Literature Review

2.1 PREVIOUS EXPERIMENTAL WORKS / RESEARCHES

Kotsovos and Leafs (1990) [3] suggested that shear failure is related to the path followed by the compression part of the bending moment. They proposed that it is the tensile stresses developed along this path, e.g. where the compression force path changes direction, which determines shear capacity of a beam. Kani (1964) [4] also demonstrated that shear strength is enhanced by poor bond.

Sharaf and Soudki (2002) [5] reported test results on seven reinforced concrete beam specimens with varying de-bonded length of reinforcement strengthened by Carbon Fiber Reinforced Polymer (CFRP) sheets. They noticed that widths of cracks in constant moment zone were considerably greater where reinforcement was de-bonded. The wider crack widths in beams with de-bonded steel are attributable to the absence of bonded reinforcement to control crack width and the increased mid-span curvature that is expected in beams with de-bonded reinforcement. Increased crack height at mid-span demonstrates a reduction in the depth of neutral axis with increasing length of exposure of reinforcement. Their investigation suggests the governing failure mode may be dependent on many parameters including bond strengthening, reinforcement ratio, concrete cover, span-to-depth ratio, bar diameter of tension reinforcement, and concrete compressive strength.

Most previous investigators explained that the flexural shear crack is simply a continuity of previously developed flexural crack, which becomes inclined with increase in load because the sections are subjected to bending as well as shear. Some investigators such as Krefeld [7] and Moody [8] reported that the flexural shear crack was distinguished from ordinary flexural cracks; the flexural shear crack was started at, or above, the tension reinforcement is inclined from its inception and it is not necessarily connected to the flexural cracks.

With increase in applied load after flexural shear cracking initiates, and in some cases this is immediately followed by member (diagonal tension) failure and in other cases the crack stabilizes and substantially more shear force can be applied before the beam fails (shear compression failure). Moreover, the horizontal cracking

(sometimes called dowel or dowel-split cracking) along the longitudinal reinforcement is conventionally considered as a secondary crack that forms after the compression zone has failed, either by disintegration or crushing.

Placing stirrups within the shear span appears to be effective in order to suppress flexural shear crack, in this case the stirrups prevent shear cracking and help increase shear capacity. This result is not compatible with the concept of a critical shear section as used in the current ACI318 shear design provisions [1].

Some of the increase in strength of the beams regarding confined horizontal cracking maybe attributed to the increase in the dowel resistance due to the external stirrup provided.

2.2 CAUSES OF SHEAR FAILURE

Kim & White (1990) [6] carried out an experimental investigation into the cause of critical-shear cracking in slender reinforced concrete beams.
The basic approach used was that the test beams were specially designed and fabricated to artificially isolate or add the effect of a certain factor on the critical-shear cracking process. Then these test results were compared with results from ordinary control beams, and the differences were analyzed to deduce the major cause for the initiation and the propagation of flexural shear cracking.
The following conclusions are based on the present experimental investigation into the flexural shear cracking behavior of slender ordinary reinforced concrete beams without web reinforcement.

1. In slender rectangular reinforced concrete beams (with no web reinforcement) failing in shear, critical shear cracking has certain common characteristics by which the process can be distinguished from ordinary flexural cracking: as shown in the Fig. [2.1(a)], shortly after onset of flexural cracking, a small inclined shear crack appears just above the longitudinal reinforcement and near the middle of the shear span. This shear crack does not necessarily originate from or connect to previously develop nearby flexural cracking. With further increase of load, the crack extends simultaneously at both ends. At one end it extends toward the loading point, and at the other it extends downward as shown in Fig. [2.1(b)].

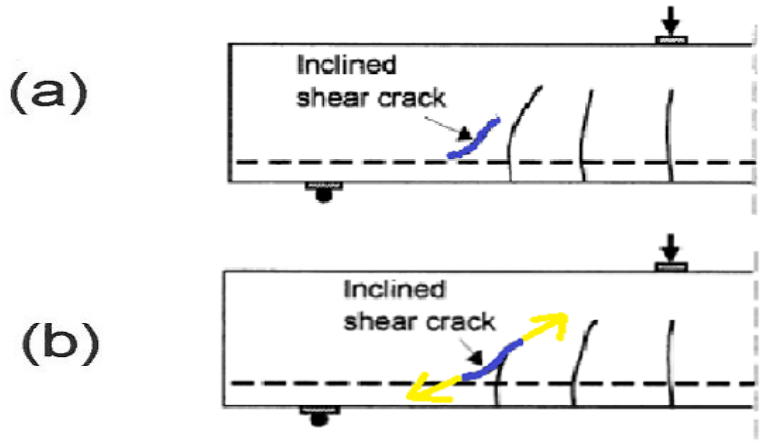

Figure 2.1: Pattern of inclined shear crack initiation observed.

2. The initiation of the critical shear cracking is found to be strongly associated with the magnification of actual shear stress produced by a distinct local stress concentration effect arising from the formation of the nearby flexural cracks. This local shear stress concentration is produced by the nature of bond between the concrete and the flexural reinforcement.

3. The stability of the critical shear cracking into the compression zone depends on the extent of the horizontal cracking along the longitudinal reinforcement. Extensive horizontal cracking produces a sudden increase of stresses at the head of the inclined shear crack and an unstable propagation mode. The primary factor for the variation of shear strengths and failure modes with respect to a_v/d is directly related to the intensity of unstable horizontal cracking.

4. Placing stirrups within the shear span beyond a distance of *2d* away from the loading point appears to be still effective in 766 ACI Structural Journal/September-October 1999 preventing shear cracking and increasing shear capacity. This result is not compatible with the concept of a critical shear section as used in the current ACI 318 shear design provisions.

5. The new concept of the bond-induced shear failure mechanism described in this paper may lead to a comprehensive understanding of the causes and mechanisms of flexural shear cracking failure in reinforced concrete beams in terms of initiation and propagation.

Chapter 3: Experimental Program

3.1 Structural form

The structural forms investigated here are simply-supported beam specimens as shown in Fig. [3.1] which also shows the specimens' cross-sectional characteristics, the load arrangement, and the relevant bending-moment and shear-force diagrams.

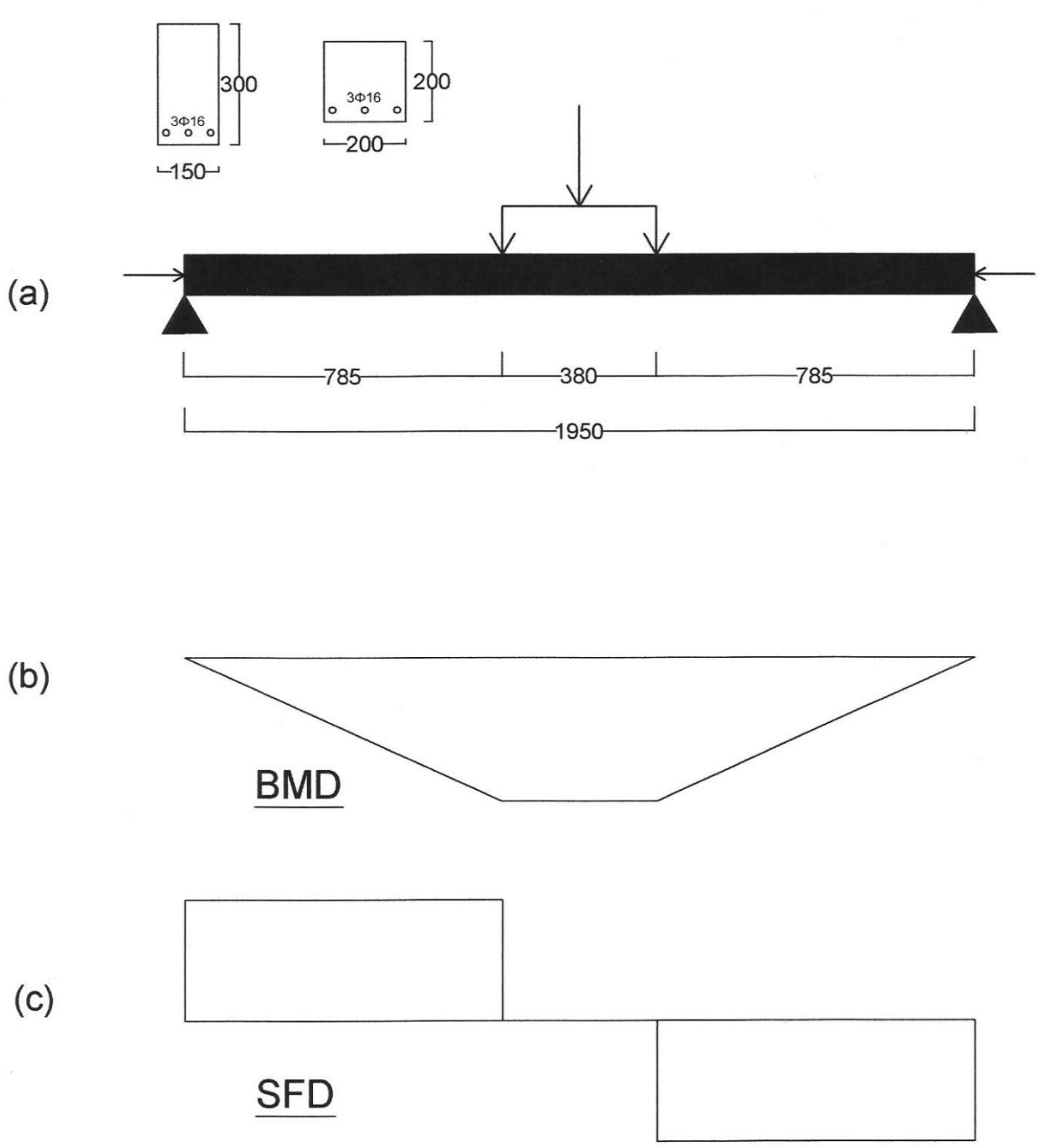

Figure 3.1: a) Structural Forms Investigated in the present work, b) Bending moment diagram, c) Shear force diagram.

From Fig. [3.1], it can be seen that the specimens had a span of 2300mm (90.55in) and 300×150mm cross sectional dimensions for rectangular and 200×200mm for square cross sections. The longitudinal reinforcement comprised three tension 16mm (0.63in) diameter deformed bars with average values of yield stress and strength equal to 575MPa (83.4ksi) and 650MPa (94.2ksi) respectively. The concrete cubic strength at the time of testing of the specimens was 28MPa (4.1ksi) at an age of approximately 2.5 months. The measured concrete cubic strength is averaged over 6 tests. The concrete strength of the cube specimens is shown in Table [3.1]. The specimens (both the control cubes and the beam elements) were cured under wet hessian for one month, after which time they were stored under laboratory ambient conditions (with a temperature of approximately $20℃$ and a relative humidity of approximately 50%).

Test	Weight (Kg)	Dimensions of Cross section (mm)	Height (mm)	Load (ton)	f_c (MPa)
1	7.55	150×150	150	78.3	34.8
2	7.45	150×150	150	72	32.0
3	7.45	150×150	150	72	32.0
4	7.45	150×150	150	76	33.8
5	7.45	150×150	150	75.8	33.7
6	7.45	150×150	150	71	31.6
Average of Compressive Strength of Concrete					33.0
Multiplied by 0.85 as reduction factor					28.0

Table 3.1: Physical characteristics, applied load and measured concrete cubic strength of 6 test beams.

3.2 Loading Path

All beams were simply supported and tested under symmetrical two-point loads which gave shear span-to-depth ratio of a_v/d = 2.9 for rectangular beams, and a_v/d = 4.6 for square beams. Two of the eight specimens were subjected to transverse loading and the other 6 were subjected to sequential loading with axial (N) and transverse (P) components, as shown in Fig. [3.2]. In the latter case, N was applied

first; it was increased to a predefined value of $N \approx 0.2\,N_u = 0.2 f_c.b.h$, where N_u is the maximum value of axial force that can be sustained by the specimen in concentric compression, f_c is the cubic compressive strength of concrete, *b* and *h* are the cross-sectional dimensions of the specimens. N_u was maintained constant with an accuracy of ±5*kN* (1.12*kpf*) during the subsequent application of *P*. The value of axial load was defined as 250kN, and then decreased to 100*kN* and 50*kN*. For all specimens tested, transverse loading was applied and increased progressively.

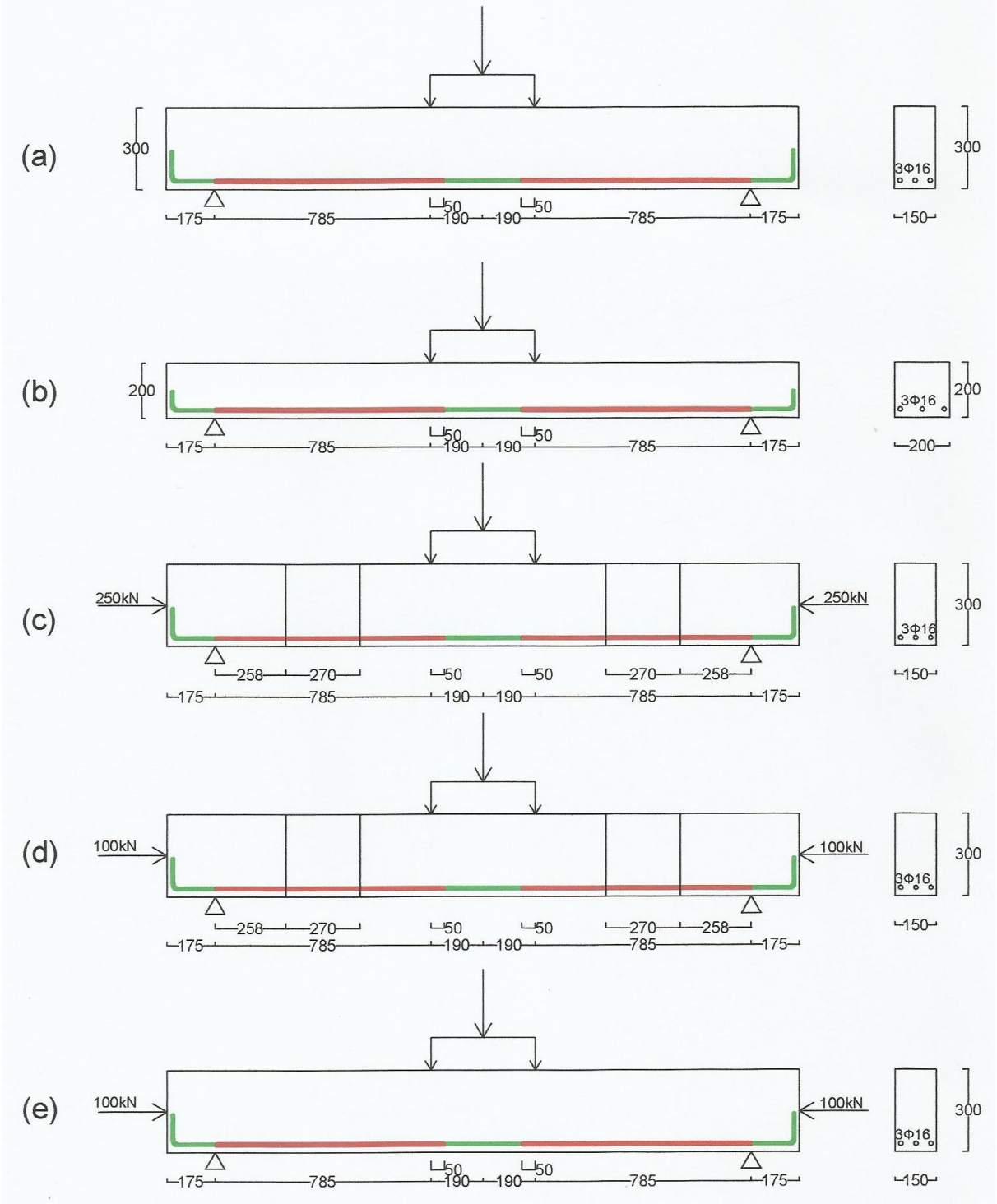

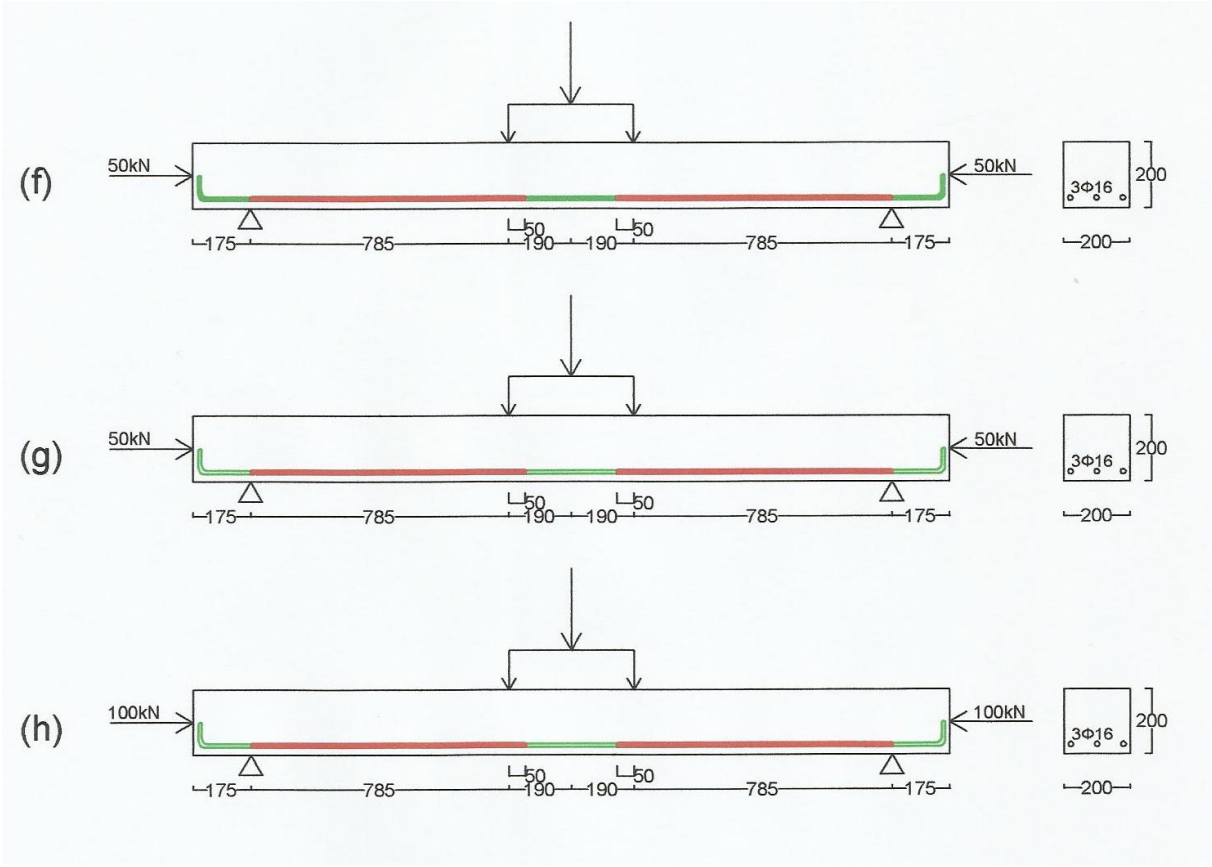

Figure 3.2: Position of load, transverse reinforcement, and cross sections of beams.

a) First beam with rectangular cross section and applied transverse load, b) Second beam with square cross section and applied transverse load, c) Third beam with rectangular cross section, transverse reinforcement and applied transverse and axial load of $250kN$, d)) Fourth beam with rectangular cross section, transverse reinforcement and applied transverse and axial load of $100kN$, e) Fifth beam with rectangular cross section and applied transverse and axial load of $100kN$, f) Sixth beam with square cross section and applied transverse and axial load of $50kN$, g) Seventh beam with square cross section and applied transverse and axial load of $50kN$, h) Eighth beam with square cross section and applied transverse and axial load of $50kN$.

3.3 Experimental set-up

The experimental arrangement used for the tests comprised two identical steel portal frames, with a double-T cross-section, bolted in parallel onto the rigid floor at a distance equal to the specimen's span. As shown in Fig. [3.3], the specimens were on roller supports positioned underneath the bottom flange of the frame beams so that the reactions could act either upwards or downwards depending on the sense of the transverse point load. The transverse load was applied at the mid span of the specimens through a double-stroke $500kN$ ($112.4kpf$) hydraulic actuator fixed to the rigid floor. The axial-compressive force was applied concentrically using an external pre-stressing force by means of four high-yield steel rods symmetrically arranged about the longitudinal axis of the specimen. The rods were anchored at each end

with two steel plates, one being attached at one end-face of the element through a load-platen arrangement ensuring concentric loading, while the other was attached at the end-face of a 900kN (202.3kpf) hydraulic actuator acting against another steel load-platen arrangement attached to the other end face of the specimen. The actuator was capable of maintaining the axial force constant with an accuracy of ±5kN (1.12kpf).

The transverse load was displacement-controlled. It was interrupted at regular intervals, corresponding to displacement increments of approximately 5mm (0.2in), during which time the load was maintained constant for at least 1min in order to mark cracks and take photographs of the specimen crack pattern. The load was measured by using a load cell, while the deformation response was measured by linear voltage differential transducers (LVDTs) measuring the deflection at the location of the transverse load point.

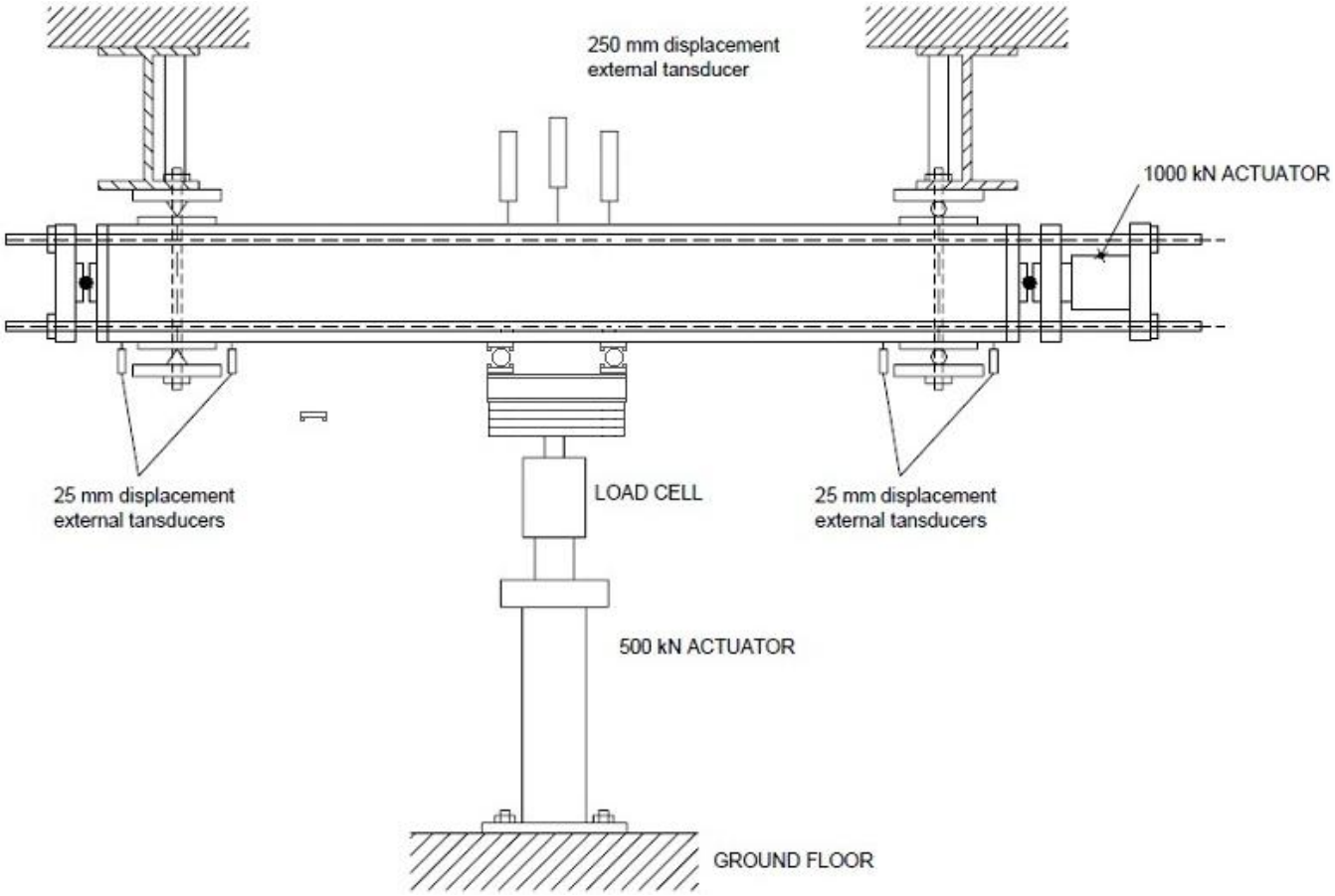

Figure 3.3: Experimental Set-up.

3.4 Specimen design

The specimens were designed with all safety factors being taken equal to 1.0 in all cases. It was assumed that load-carrying capacity is reached when the specimen attains its flexural capacity, the latter condition being referred to as plastic-hinge formation. Using the cross-sectional and material characteristics of the specimens, together with a rectangular compressive-stress block with a depth equal to the neutral-axis depth and a stress intensity equal to f_c, as recommended by the CFP Method, the flexural capacity of the specimen was calculated as M_f (for a value of N equal to $N \approx aN_u$, with an obtaining values equal to 0.0 or 0.2 corresponding to values of N equal to $0kN$ and $250kN$ respectively).

Chapter 4: Transverse Reinforcement Design

The transverse reinforcement was designed for rectangular cross section beams in two cases of applied axial force and one without axial force based on CFP Method. Figs. [4.1] and [4.2] show the CFP in two cases of beam without applied axial force and with axial force, respectively.

For designing transverse reinforcement for the beam without applied force, From Fig. [4.1], we have:

From Δ ABB′;

$$\propto = tan^{-1}\left(\frac{BB'}{AB'}\right) = tan^{-1}\left(\frac{270}{785}\right) = 19.0°$$

$$F_s = A_s.f_y = \frac{3(\pi \times 16^2)}{4} \times 575 = 3.5 \times 10^5 N$$

$$F_c = \frac{F_s}{cos\ (\alpha)} = \frac{3.5 \times 10^5}{cos\ (19.0)} = 3.7 \times 10^5 N$$

$From\ \Delta\ OCD;$

$$OC = \frac{d}{2} = \frac{270}{2} = 135mm$$

$$OD = \frac{OC}{cos\ (\alpha)} = \frac{135}{cos\ (19.0)} = 143mm$$

From Δ AOD;

$$\omega = \alpha = 19.0°$$

$$T' = F_c\,.tan(\omega) = 3.7 \times 10^5 \times tan(19.0) = 1.3 \times 10^5 N$$

From Δ OCD;

$$T_s = T'.cos\ (\alpha) = 1.3 \times 10^5 \times cos(19.0) = 1.2 \times 10^5 N$$

$$A_s = \frac{T_s}{f_y} = \frac{1.2 \times 10^5}{575} = 207.5\ mm^2$$

Two two-legged stirrups dia.12mm were used.

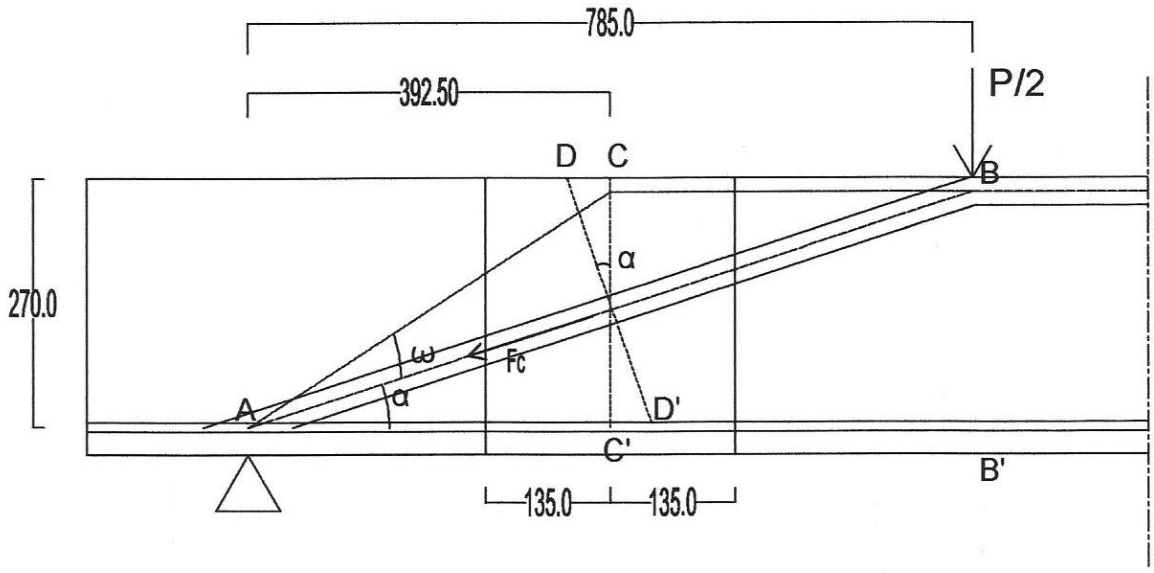

Figure 4.1: Transverse Reinforcement design for beam without axial load.

For designing transverse reinforcement for the beam with applied force, From Fig. [4.2], we have:

$F_s = 3.5 \times 10^5 N$

$N = 0.2.F_c.A = 0.2 \times 28 \times 150 \times 300 = 2.52 \times 10^5 N$

$R = F_s + N = 3.5 \times 10^5 + 2.52 \times 10^5 = 6.0 \times 10^5 N$

$R.x_2 = N.x_1 + f_s.x_3$

$$x_2 = \frac{2.52 \times 10^5 \times 150 + 3.5 \times 10^5 \times 30}{6.0 \times 10^5} = 80.5mm$$

From Δ AOC′;

$$\alpha = tan^{-1}\left(\frac{300 - 80.5}{785}\right) = 15.6$$

$$f_c = \frac{R}{cos\ (\alpha)} = \frac{6.0 \times 10^5}{cos(15.6)} = 6.2 \times 10^5 N$$

From Δ AOD;

$\omega = \alpha = 15.6$

$T' = f_c\ .tan\ (\omega) = 6.2 \times 10^5 \times tan(15.62) = 1.7 \times 10^5 N$

From Δ OCD;

$T_s = T'.cos\ (\alpha) = 1.7 \times 10^5 N \times cos(15.6) = 1.7 \times 10^5 N$

$$A_s = \frac{T_s}{f_y} = \frac{1.7 \times 10^5}{575} = 291.2\ mm^2$$

Two two-legged stirrups dia.12mm were used.

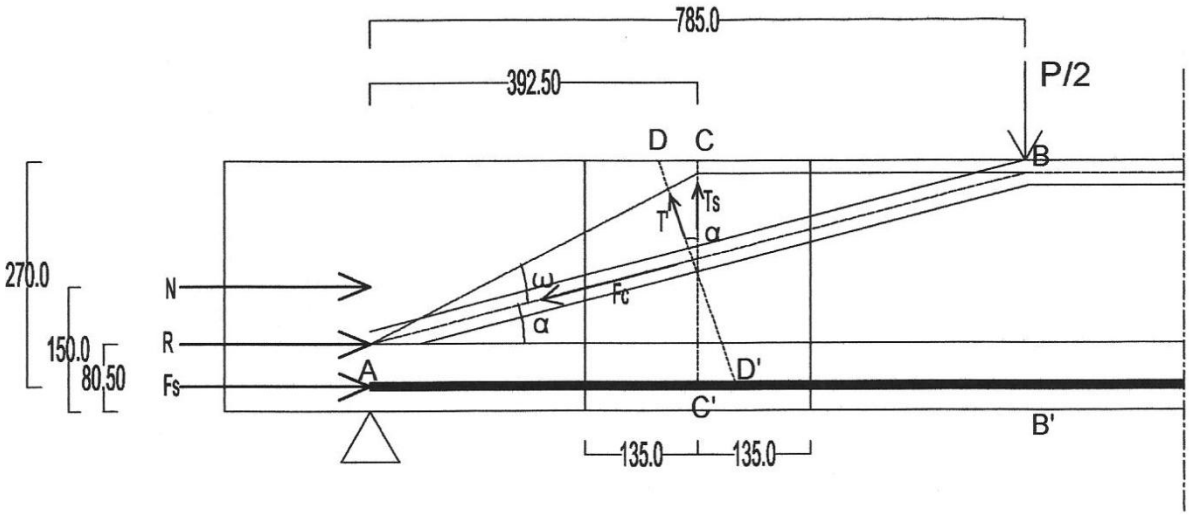

Figure 4.2: Transverse Reinforcement design for beam with axial load.

Chapter 5: Data Results and Analysis

5.1 Data

5.1.1 First Test Beam

Fig. [5.1] shows the crack pattern in the first test beam. As it can be seen, the cracks mostly include flexural cracks in the mid span of the beam and a crack also forms in the shear span which is a post tension crack that when the load reduces by up to 20% to 30% after it reaches the peak point, a crack forms from point load to the support.

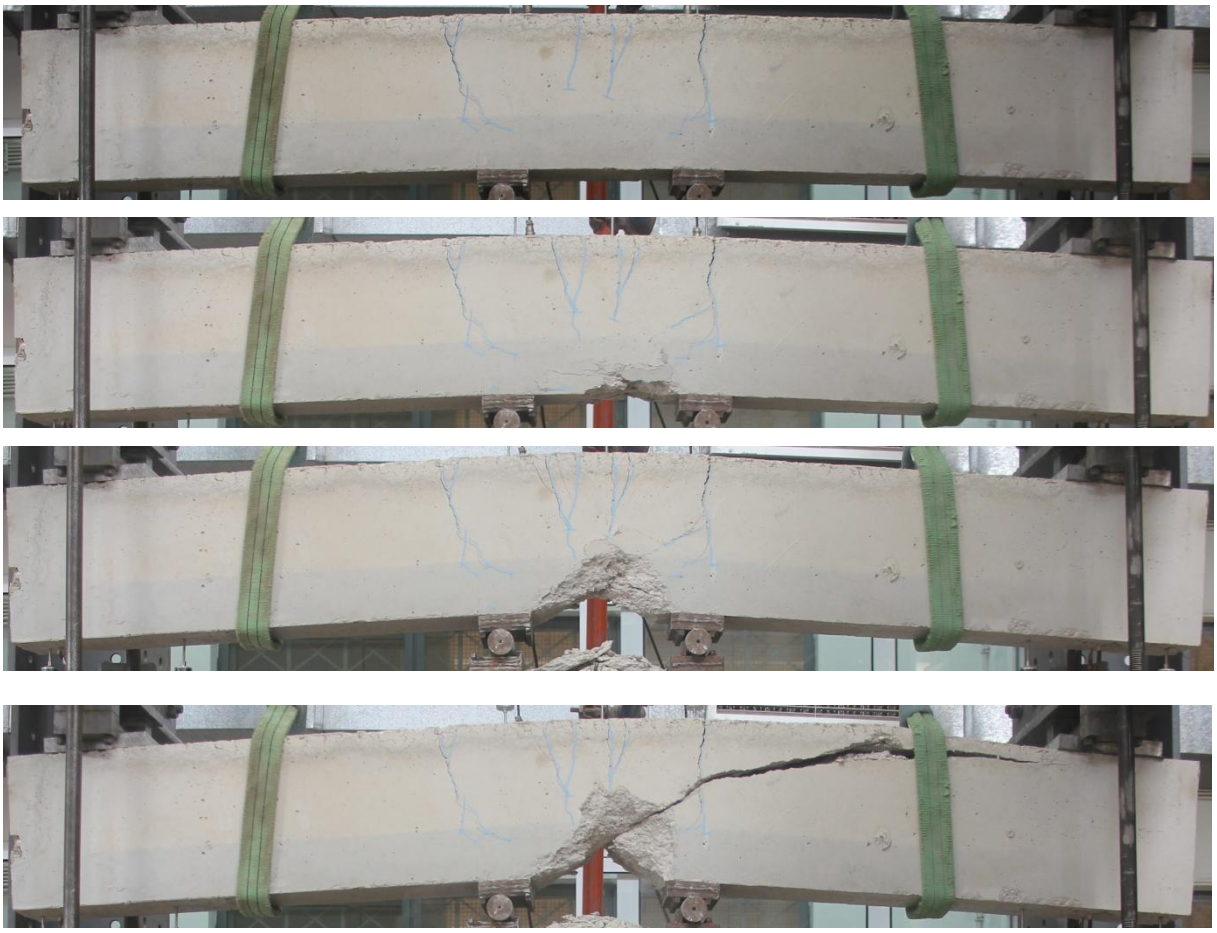

Figure 5.1: Crack pattern in the first beam.

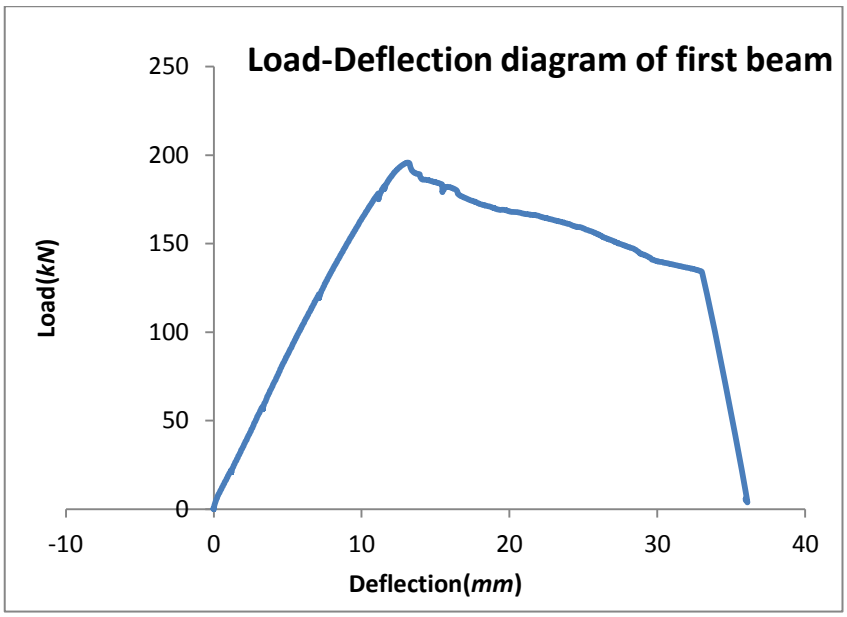

Figure 5.2: Load-deflection diagram of the first beam.

5.1.2 Second Test Beam

For the second test beam, the cracks are shown in Fig.[5.3]. The cracks are mostly flexural in the mid span of the beam, and also a post tension crack which is in the shear span from point load to the support.

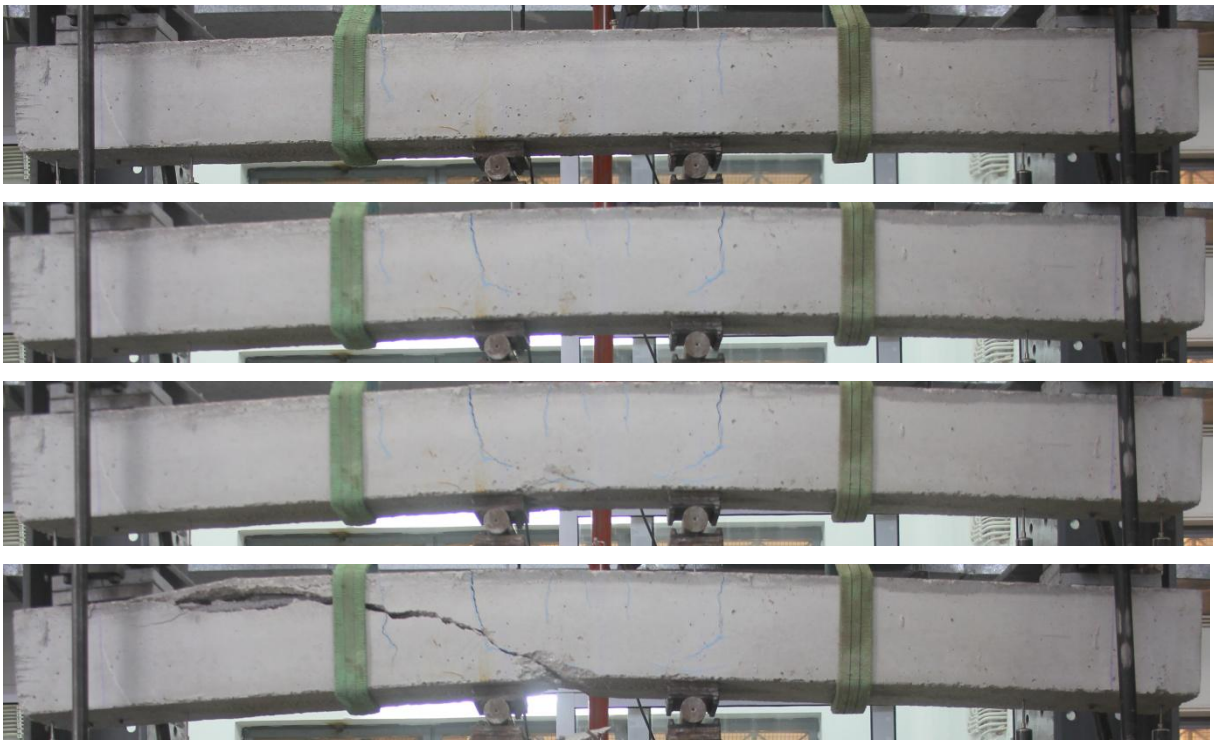

Figure 5.3: Crack pattern of the second beam.

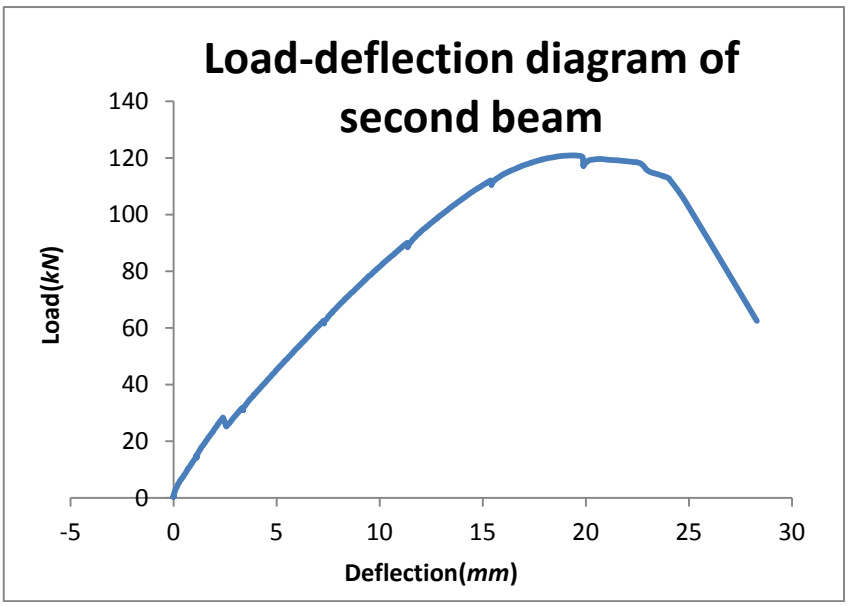

Figure 5.4: Load-deflection diagram of the second beam.

5.1.3 Third Test Beam

For the third test beam, as it is shown in below figures, the beam is reinforced by four stirrups which are placed in the shear span, and an axial load of 250kN is applied on the end of the beam. The flexural cracks in the mid-span of the beam are shown in figures [5.5].

Figure 5.5: Crack pattern of the third beam.

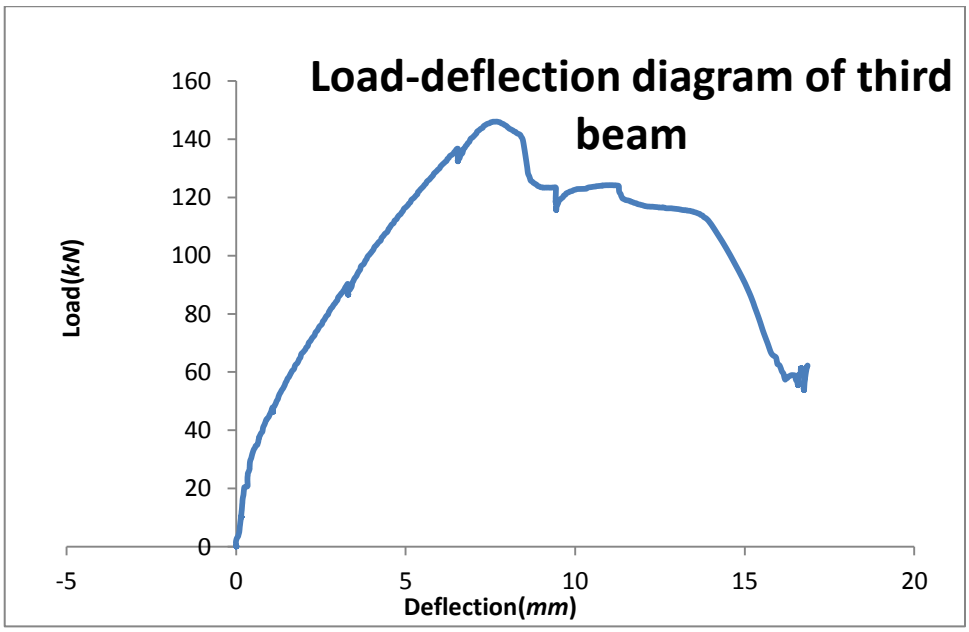

Figure 5.6: Load-deflection diagram of the third beam.

5.1.4 Fourth Test Beam

The same as third test beam, the fourth beam is also reinforced with four stirrups that are placed in the shear span of the beam, and the axial load is reduced to $100kN$ which is applied on the end of the beam. As it can be seen in Fig.[5.7], flexural cracks are formed in the mid-span of the beam.

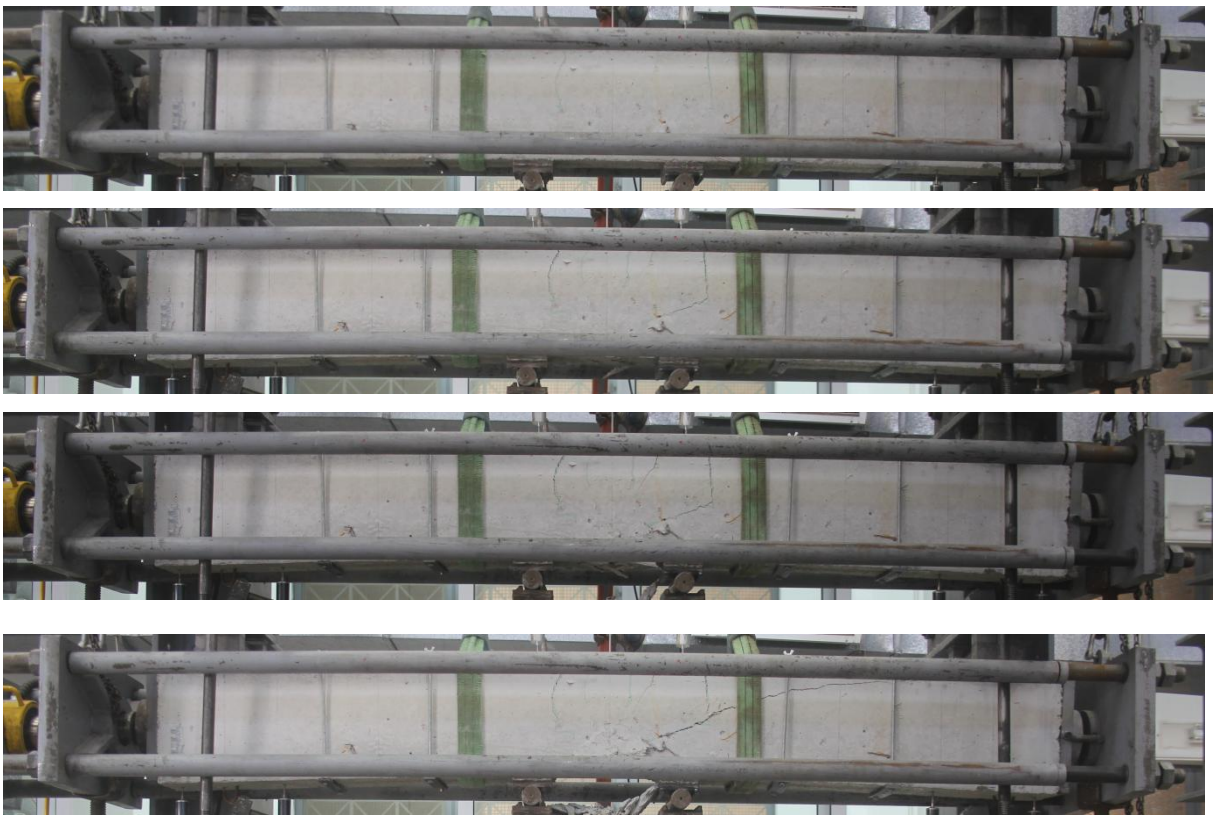

Figure 5.7: Crack pattern of the fourth beam.

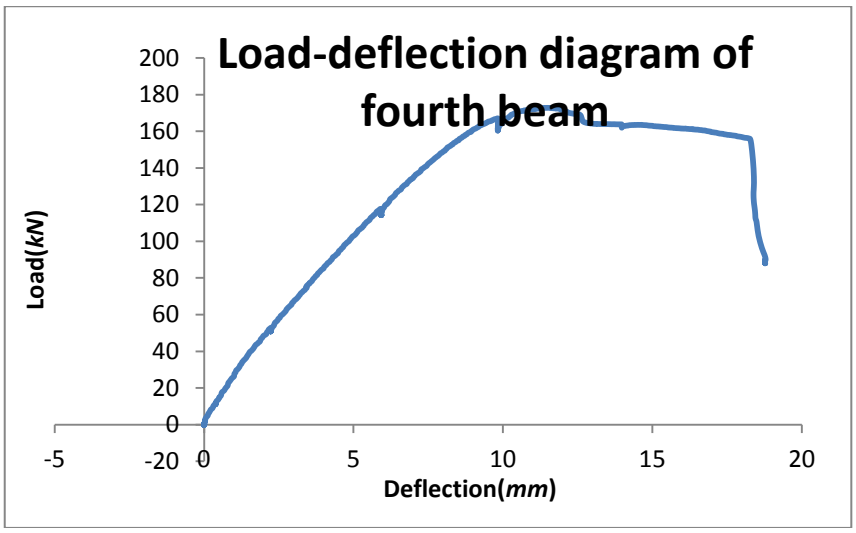

Figure 5.8: Load-deflection diagram of the fourth beam.

5.1.5 Fifth Test Beam

The same as fourth beam, the axial load of 100kN is applied on the beam, but the beam is not reinforced with stirrups. As it can be seen in Fig.[5.9], flexural cracks are formed in the mid-span and the beam is failed in the mid-span.

Figure 5.9: Crack pattern of the fifth beam.

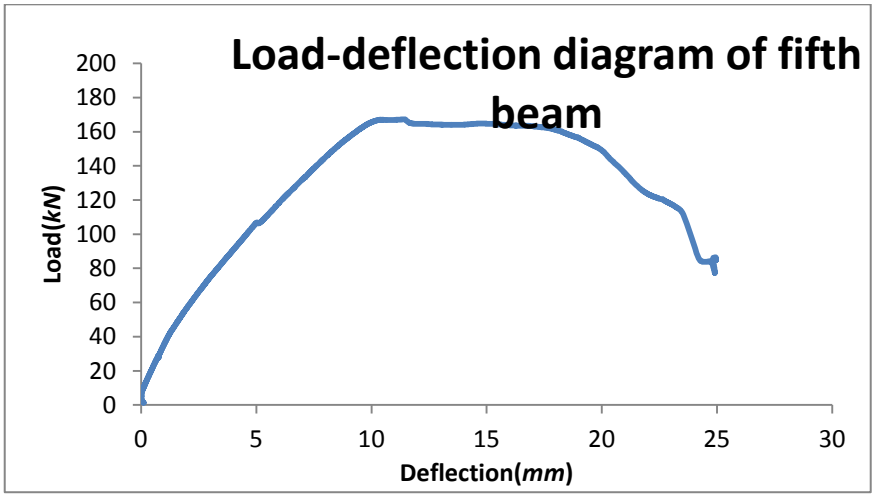

Figure 5.10: Load-deflection diagram of the fifth beam.

5.1.6 Sixth Test Beam

For the sixth beam, the cross section is square and axial load is reduced to $50kN$, and the beam is not reinforced with stirrups. As it can be seen in Fig. [5.11], flexural cracks are formed within the mid-span, and also a post tension crack which is formed within the shear span of the beam.

Figure 5.11: Crack pattern of the sixth beam.

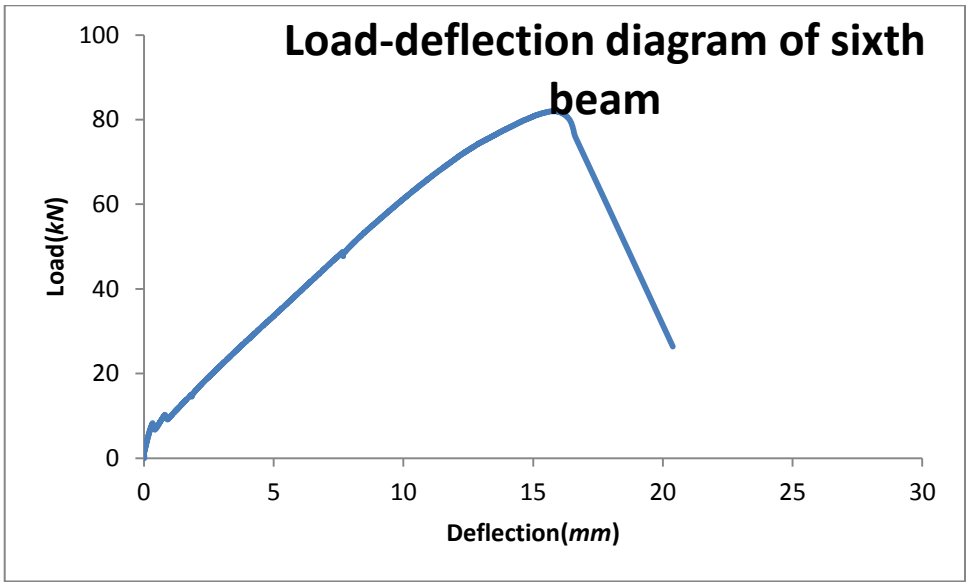

Figure 5.12: Load-deflection diagram of the sixth beam.

5.1.7 Seventh Test Beam

For the seventh beam, also the same as sixth beam the cross section is square and axial load is 50KN, and the beam is not reinforced with stirrups.

Figure 5.13: Crack pattern of the seventh beam.

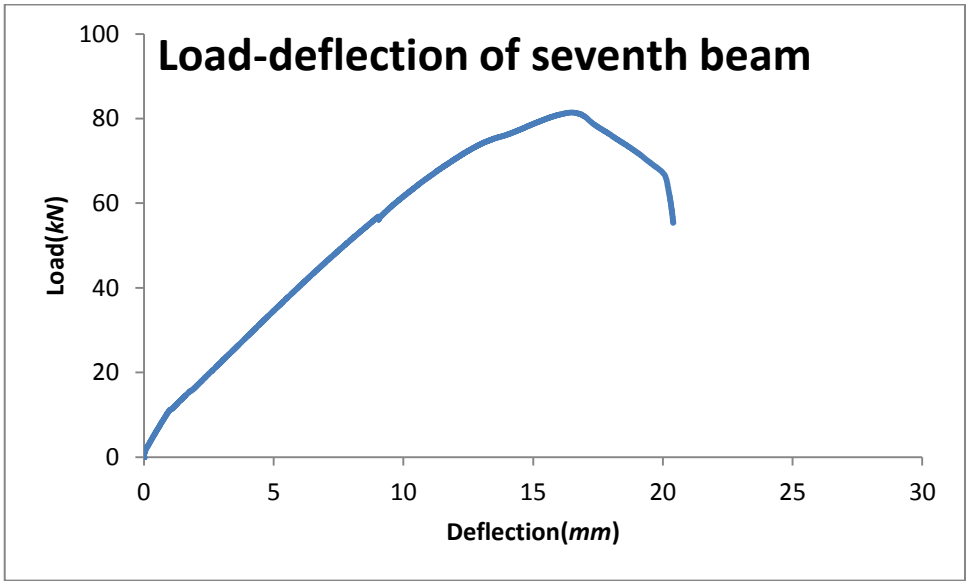

Figure 5.14: Load-deflection diagram of the seventh beam.

5.1.8 Eighth Test Beam

For the eighth beam, the cross section is square, and the axial load of $100kN$ is applied on the beam, and the beam is not reinforced with stirrups.

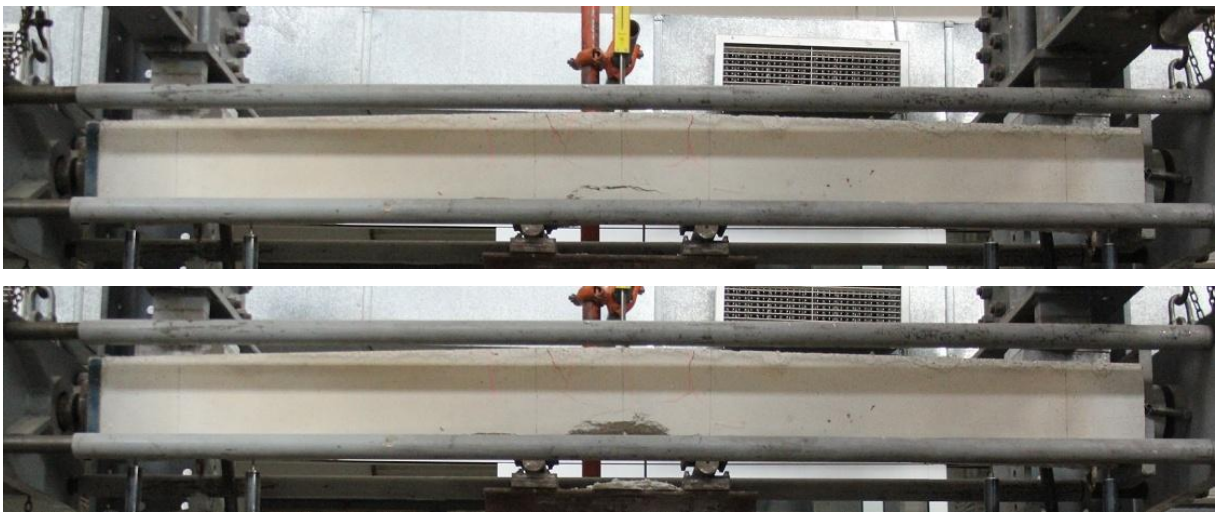

Figure 5.15: Crack pattern of the eighth beam.

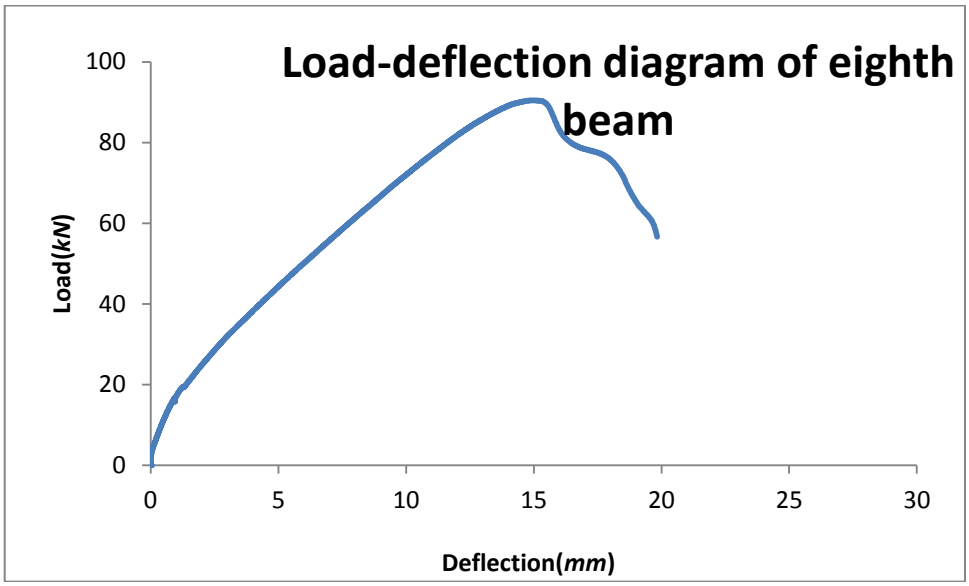

Figure 5.16: Load-deflection diagram of the eighth beam.

5.1.9 Calculated Values of Nominal Bending Moment and Load Carrying Capacity

For each beam specimen, the values of the nominal load and bending moment are calculated. By using M_f, the specimens' load-carrying capacity $P_f = 4\,M_f\,/L$ (where L is the specimens' span) and, hence, the corresponding shear force $V_f = P_f\,/2$ is calculated.

5.1.9.1 First Beam

$h = 300\,mm, \qquad b = 150\,mm, \qquad d = 300 - 30 = 270\,mm$

$F_c = F_s \quad \Rightarrow \quad f_c.b.x = A_s.f_y$

$$28 \times 150 \times x = 3 \times (\frac{\pi \times 16^2}{4}) \times 575$$

$$x = 82.6mm$$

$$z = 270 - \frac{82.6}{2} = 228.7mm$$

$$M_f = F_c.z = 28 \times 150 \times 82.6 \times 228.7 = 79.3kN.m$$

$$M_f = \frac{P_f \times a_v}{2} \Rightarrow 79.3 \times 10^6 = \frac{P_f \times 785}{2} \quad \Rightarrow \quad P_f = 202.1kN$$

$$V_f = 101.1\,kN$$

5.1.9.2 Second Beam

$h = 200mm, \qquad b = 200mm, \qquad d = 200 - 30 = 170mm$

$F_c = F_s \quad \Rightarrow \quad f_c.b.x = A_s.f_y$

$$28 \times 200 \times x = 3 \times (\frac{\pi \times 16^2}{4}) \times 575$$

$$x = 61.9mm$$

$$z = 170 - \frac{61.9}{2} = 139.0mm$$

$$M_f = F_c.z = 28 \times 200 \times 61.9 \times 139.0 = 48.2kN.m$$

$$M_f = \frac{P_f \times a_v}{2} \Rightarrow 48.2 \times 10^6 = \frac{P_f \times 785}{2} \quad \Rightarrow \quad P_f = 122.9kN$$

$V_f = 61.4kN$

5.1.9.3 Third Beam

$h = 300mm\,,\qquad b = 150mm,\qquad d = 300 - 30 = 270mm$

$N = 28 \times 0.2 \times 150 \times 300 = 2.5 \times 10^5 kN$

$F_c - F_s = N \quad \Rightarrow \quad f_c.b.x - A_s.f_y = N$

$$28 \times 150 \times x - 3 \times \left(\frac{\pi \times 16^2}{4}\right) \times 575 = 2.5 \times 10^5$$

$x = 142.6mm$

$$M_f = F_c\left(\frac{h}{2} - \frac{x}{2}\right) + (F_c - N)\left(\frac{h}{2} - d'\right)$$

$$= 28 \times 150 \times 142.6\left(\frac{300}{2} - \frac{142.6}{2}\right) + (28 \times 150 \times 142.6 - 2.5 \times 10^5)$$

$$\times \left(\frac{300}{2} - 30\right) = 88.8kN.m$$

$$M_f = \frac{P_f \times a_v}{2} \Rightarrow 88.8 \times 10^6 = \frac{P_f \times 785}{2} \quad \Rightarrow \quad P_f = 226.1kN$$

$V_f = 113.1kN$

5.1.9.4 Fourth Beam

$h = 300mm,\qquad b = 150mm,\qquad d = 300 - 30 = 270mm$

$N = 100kN$

$F_c - F_s = N \quad \Rightarrow \quad f_c.b.x - A_s.f_y = N$

$$28 \times 150 \times x - 3 \times \left(\frac{\pi \times 16^2}{4}\right) \times 575 = 1.0 \times 10^5$$

$x = 106.4mm$

$$M_f = F_c\left(\frac{h}{2}-\frac{x}{2}\right)+(F_c-N)\left(\frac{h}{2}-d'\right)$$

$$= 28\times150\times106.4\left(\frac{300}{2}-\frac{106.4}{2}\right)+(28\times150\times106.4-1.0\times10^5)$$

$$\times(\frac{300}{2}-30)=84.9kN.m$$

$$M_f=\frac{P_f\times a_v}{2}\Rightarrow 84.9\times10^6=\frac{P_f\times785}{2} \quad \Rightarrow \quad P_f=216.2kN$$

$$V_f=108.1kN$$

5.1.9.5 Fifth Beam

$$h=300mm, \qquad b=150mm, \qquad d=300-30=270mm$$

$$N=100kN$$

$$F_c-F_s=N \quad \Rightarrow \quad f_c.b.x-A_s.f_y=N$$

$$28\times150\times x-3\times\left(\frac{\pi\times16^2}{4}\right)\times575=1.0\times10^5$$

$$x=106.4mm$$

$$M_f = F_c\left(\frac{h}{2}-\frac{x}{2}\right)+(F_c-N)\left(\frac{h}{2}-d'\right)$$

$$= 28\times150\times106.4\left(\frac{300}{2}-\frac{106.4}{2}\right)+(28\times150\times106.4-1.0\times10^5)$$

$$\times(\frac{300}{2}-30)=84.9kN.m$$

$$M_f=\frac{P_f\times a_v}{2}\Rightarrow 84.9\times10^6=\frac{P_f\times785}{2} \quad \Rightarrow \quad P_f=216.2kN$$

$$V_f=108.1kN$$

5.1.9.6 Sixth Beam

$$h=200mm, \qquad b=200mm, \qquad d=200-30=170mm$$

$$N=50kN$$

$$F_c-F_s=N \quad \Rightarrow \quad f_c.b.x-A_s.f_y=N$$

$$28 \times 200 \times x - 3 \times \left(\frac{\pi \times 16^2}{4}\right) \times 575 = 5 \times 10^4$$

$$x = 70.9mm$$

$$M_f = F_c\left(\frac{h}{2} - \frac{x}{2}\right) + (F_c - N)\left(\frac{h}{2} - d'\right)$$

$$= 28 \times 200 \times 70.9\left(\frac{200}{2} - \frac{70.9}{2}\right) + (28 \times 200 \times 70.9 - 5 \times 10^4) \times (\frac{200}{2}$$

$$- 30) = 49.9kN.m$$

$$M_f = \frac{P_f \times a_v}{2} \Rightarrow 49.9 \times 10^6 = \frac{P_f \times 785}{2} \quad \Rightarrow \quad P_f = 127.1kN$$

$$V_f = 63.6kN$$

5.1.9.7 Seventh Beam

$$h = 200mm, \qquad b = 200mm, \qquad d = 200 - 30 = 170mm$$

$$N = 50kN$$

$$F_c - F_s = N \quad \Rightarrow \quad f_c.b.x - A_s.f_y = N$$

$$28 \times 200 \times x - 3 \times \left(\frac{\pi \times 16^2}{4}\right) \times 575 = 5.0 \times 10^4$$

$$x = 70.9mm$$

$$M_f = F_c\left(\frac{h}{2} - \frac{x}{2}\right) + (F_c - N)\left(\frac{h}{2} - d'\right)$$

$$= 28 \times 200 \times 70.9\left(\frac{200}{2} - \frac{70.9}{2}\right) + (28 \times 200 \times 70.9 - 5.0 \times 10^4) \times (\frac{200}{2}$$

$$- 30) = 49.9kN.m$$

$$M_f = \frac{P_f \times a_v}{2} \Rightarrow 49.9 \times 10^6 = \frac{P_f \times 785}{2} \quad \Rightarrow \quad P_f = 127.1kN$$

$$V_f = 63.6kN$$

5.1.9.8 Eighth Beam

$h = 200mm, \qquad b = 200mm, \qquad d = 200 - 30 = 170mm$

$N = 100kN$

$F_c - F_s = N \quad \Rightarrow \quad f_c.b.x - A_s.f_y = N$

$$28 \times 200 \times x - 3 \times \left(\frac{\pi \times 16^2}{4}\right) \times 575 = 1.0 \times 10^5$$

$x = 79.8mm$

$$M_f = F_c\left(\frac{h}{2} - \frac{x}{2}\right) + (F_c - N)\left(\frac{h}{2} - d'\right)$$

$$= 28 \times 200 \times 79.8\left(\frac{200}{2} - \frac{79.8}{2}\right) + (28 \times 200 \times 79.8 - 1.0 \times 10^5) \times (\frac{200}{2} - 30) = 51.1kN.m$$

$$M_f = \frac{P_f \times a_v}{2} \Rightarrow 51.1 \times 10^6 = \frac{P_f \times 785}{2} \quad \Rightarrow \quad P_f = 130.3kN$$

$V_f = 65.1kN$

5.1.10 Tensile Stress in Longitudinal Reinforcement

For every specimen beam, tensile stress of longitudinal reinforcement is calculated in order to check if they have yielded or not. For each beam, the value of P_{exp} is obtained from the maximum load which can be carried by the beam in experiment. The value of V_{exp} is the half of P_{exp}.

5.1.10.1 First Beam

$P_{exp} = 195.8kN,$ $V_{exp} = 97.9kN$

$M_{exp} = V.a_v = 97.9 \times 10^3 \times 785 = 76.9kN.m$

$F_c.z = M_{exp} \Rightarrow 28 \times 150 \times x\left(270 - \frac{x}{2}\right) = 76.9 \times 10^6$

$x = 79.5mm$

$F_c = F_s$

$28 \times 150 \times 79.5 = 3 \times \frac{\pi}{4} \times 16^2 \times f_s \Rightarrow f_s = 553MPa$

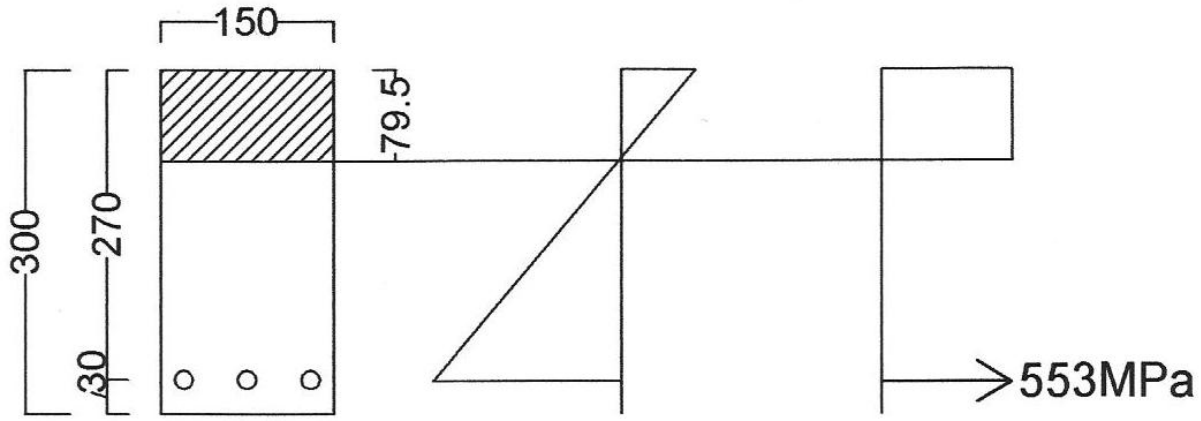

Figure 5.17: Stress and strain diagram of the first beam.

5.1.10.2 Second Beam

$P_{exp} = 120.9kN, \qquad V_{exp} = 60.4kN$

$M_{exp} = V.a_v = 60.4 \times 10^3 \times 785 = 47.4kN.m$

$F_c.z = M_{exp} \quad \Rightarrow \quad 28 \times 200 \times x\left(170 - \frac{x}{2}\right) = 47.4 \times 10^6$

$x = 60.7mm$

$F_c = F_s$

$28 \times 200 \times 60.66 = 3 \times \frac{\pi}{4} \times 16^2 \times f_s \quad \Rightarrow \quad f_s = 563MPa$

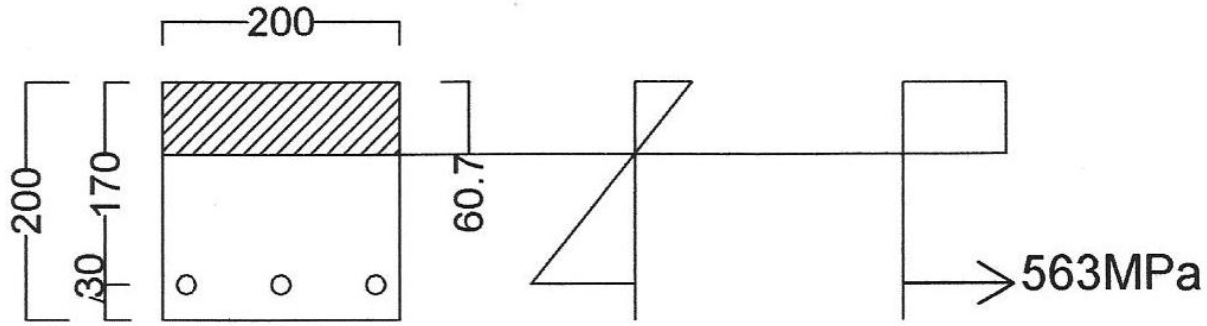

Figure 5.18: Stress and strain diagram of the second beam.

5.1.10.3 Third Beam

$P_{exp} = 146.0kN, \qquad V_{exp} = 73.0kN$

$M_{exp} = V.a_v = 73.0 \times 10^3 \times 785 = 57.3kN.m$

$M_{exp} = F_c\left(\frac{h}{2} - \frac{x}{2}\right) + (F_c - N)\left(\frac{h}{2} - d'\right)$

$28 \times 150x\left(\frac{300}{2} - \frac{x}{2}\right) + (28 \times 150x - 2.5 \times 10^5) \times \left(\frac{300}{2} - 30\right) - 57.3 \times 10^6 = 0$

$-2.1 \times 10^3.x^2 + 1.1 \times 10^6.x - 8.8 \times 10^7 = 0$

$x = 93.3mm$

$F_s = 28 \times 150 \times 93.3 - 2.5 \times 10^5 = 1.4 \times 10^5$

$1.4 \times 10^5 = 3 \times \frac{\pi}{4} \times 16^2 \times f_s \quad \Rightarrow \quad f_s = 232MPa$

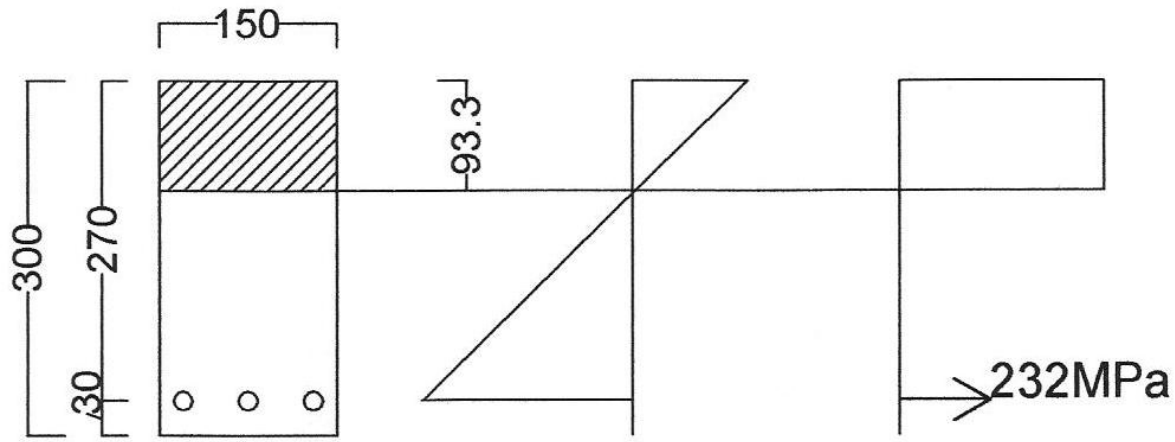

Figure 5.19: Stress and strain diagram of the third beam.

5.1.10.4 Fourth Beam

$P_{exp} = 172.8kN, \qquad V_{exp} = 86.4kN$

$M_{exp} = V.a_v = 86.4 \times 0.785 = 67.8kN.m$

$M_{exp} = F_c\left(\frac{h}{2} - \frac{x}{2}\right) + (F_c - N)\left(\frac{h}{2} - d'\right)$

$28 \times 150x\left(\frac{300}{2} - \frac{x}{2}\right) + (28 \times 150x - 1.0 \times 10^5) \times \left(\frac{300}{2} - 30\right) - 67.8 \times 10^6 = 0$

$-2.1 \times 10^3.x^2 + 1.1 \times 10^6.x - 8.0 \times 10^7 = 0$

$x = 83.2mm$

$F_s = 28 \times 150 \times 83.2 - 1.0 \times 10^5 = 2.5 \times 10^5$

$2.5 \times 10^5 = 3 \times \frac{\pi}{4} \times 16^2 \times f_s \quad \Rightarrow \quad f_s = 414MPa$

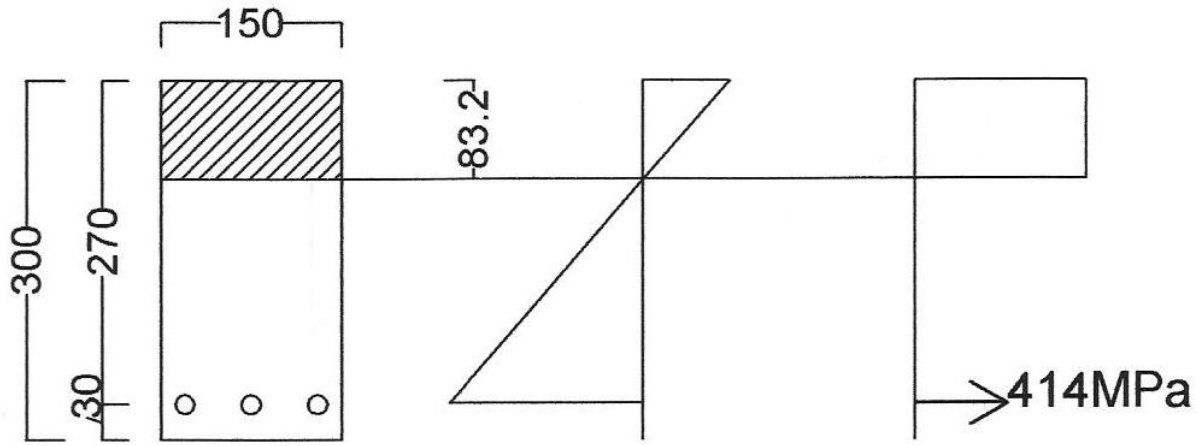

Figure 5.20: Stress and strain diagram of the fourth beam.

5.1.10.5 Fifth Beam

$P_{exp} = 167.3kN, \qquad V_{exp} = 83.7kN$

$M_{exp} = V.a_v = 83.7 \times 10^3 \times 785 = 65.7kN.m$

$M_{exp} = F_c\left(\frac{h}{2} - \frac{x}{2}\right) + (F_c - N)\left(\frac{h}{2} - d'\right)$

$28 \times 150x\left(\frac{300}{2} - \frac{x}{2}\right) + (28 \times 150x - 1.0 \times 10^5) \times \left(\frac{300}{2} - 30\right) - 65.7 \times 10^6 = 0$

$-2.1 \times 10^3.x^2 + 1.1 \times 10^6.x - 7.8 \times 10^7 = 0$

$x = 80.5mm$

$F_s = 28 \times 150 \times 80.5 - 1.0 \times 10^5 = 2.4 \times 10^5$

$2.4 \times 10^5 = 3 \times \frac{\pi}{4} \times 16^2 \times f_s \quad \Rightarrow \quad f_s = 395MPa$

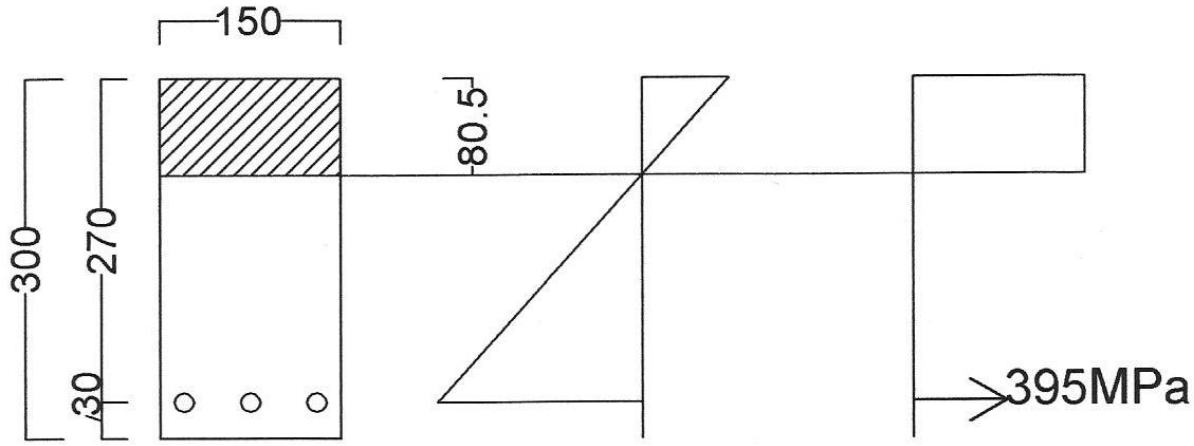

Figure 5.21: Stress and strain diagram of the fifth beam.

5.1.10.6 Sixth Beam

$P_{exp} = 82.0kN, \qquad V_{exp} = 41.0kN$

$M_{exp} = V.a_v = 41.0 \times 10^3 \times 785 = 32.2kN.m$

$M_{exp} = F_c\left(\frac{h}{2} - \frac{x}{2}\right) + (F_c - N)\left(\frac{h}{2} - d'\right)$

$28 \times 200x\left(\frac{200}{2} - \frac{x}{2}\right) + (28 \times 200x - 5 \times 10^4) \times \left(\frac{200}{2} - 30\right) - 32.2 \times 10^6 = 0$

$-2.8 \times 10^3.x^2 + 9.5 \times 10^5.x - 3.6 \times 10^7 = 0$

$x = 42.9mm$

$F_s = 28 \times 200 \times 42.9 - 5 \times 10^4 = 1.9 \times 10^5$

$1.9 \times 10^5 = 3 \times \frac{\pi}{4} \times 16^2 \times f_s \quad \Rightarrow \quad f_s = 315MPa$

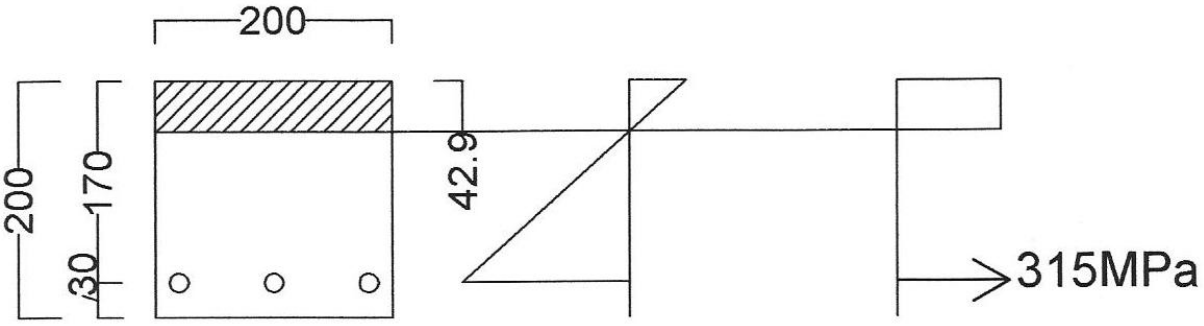

Figure 5.22: Stress and strain diagram of the seventh beam.

5.1.10.7 Seventh Beam

$P_{exp} = 81.4kN, \qquad V_{exp} = 40.7kN$

$M_{exp} = V.a_v = 40.7 \times 10^3 \times 785 = 32.0kN.m$

$M_{exp} = F_c\left(\frac{h}{2} - \frac{x}{2}\right) + (F_c - N)\left(\frac{h}{2} - d'\right)$

$28 \times 200x\left(\frac{200}{2} - \frac{x}{2}\right) + (28 \times 200x - 5 \times 10^4) \times \left(\frac{200}{2} - 30\right) - 3.2 \times 10^7 = 0$

$-2.8 \times 10^3.x^2 + 9.5 \times 10^5.x - 3.5 \times 10^7 = 0$

$x = 42.6mm$

$F_s = 28 \times 200 \times 42.6 - 5 \times 10^4 = 1.9 \times 10^5$

$1.9 \times 10^5 = 3 \times \frac{\pi}{4} \times 16^2 \times f_s \quad \Rightarrow \quad f_s = 313MPa$

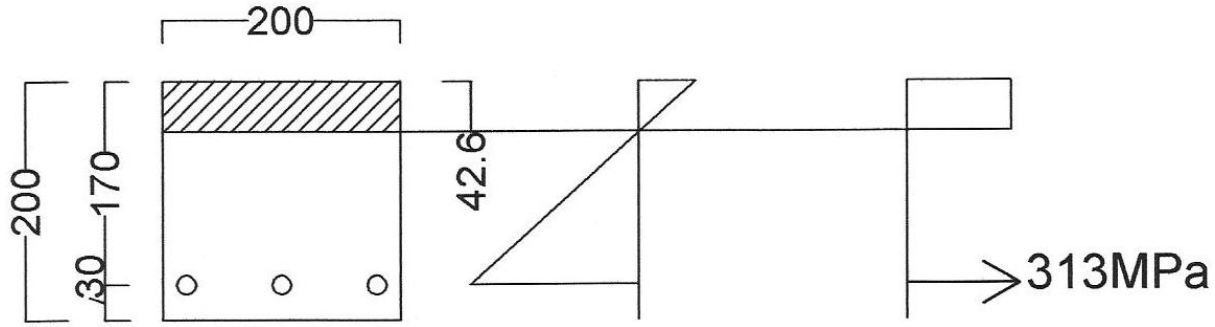

Figure 5.23: Stress and strain diagram of the sixth beam.

5.1.10.8 Eighth Beam

$P_{exp} = 90.5kN, \qquad V_{exp} = 45.2kN$

$M_{exp} = V.a_v = 45.2 \times 10^3 \times 785 = 35.5kN.m$

$M_{exp} = F_c\left(\frac{h}{2} - \frac{x}{2}\right) + (F_c - N)\left(\frac{h}{2} - d'\right)$

$28 \times 200x\left(\frac{200}{2} - \frac{x}{2}\right) + (28 \times 200x - 1.0 \times 10^5) \times \left(\frac{200}{2} - 30\right) - 35 \times 10^6 = 0$

$-2.8 \times 10^3.x^2 + 9.5 \times 10^5.x - 4.3 \times 10^7 = 0$

$x = 52.9mm$

$F_s = 28 \times 200 \times 52.87 - 1.0 \times 10^5 = 2.0 \times 10^5$

$2.0 \times 10^5 = 3 \times \frac{\pi}{4} \times 16^2 \times f_s \quad \Rightarrow \quad f_s = 325MPa$

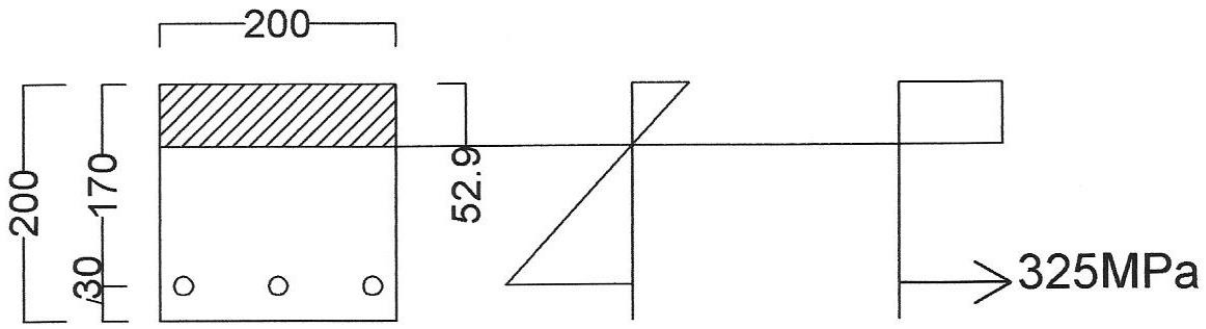

Figure 5.24: Stress and strain diagram of the eighth beam.

5.2 Results and Analysis

By applying load, flexural cracks form in the mid-span of beam and then shear crack forms independently from flexural cracks. With further increase in load, the crack propagates simultaneously from both ends. One end extends toward the loading point, and the other end extends toward the support.

The formation of shear crack is found to be strongly dependent on the concentration of shear stress which is formed slightly above the reinforcement and near the outermost flexural crack. This shear stress is produced because of the bond between concrete and flexural reinforcement. With no bond between the concrete and reinforcement in the shear span, this local shear stress concentration does not form, and as a result the shear cracks are prevented.

In previous researches, the aim has been to find the length and position of de-bonded reinforcement in order to prevent cracks in the shear span. As it is seen in all test beams, by removing the bond between longitudinal reinforcement and concrete, the beam does not fail in shear. The cracks in the beams are all flexural cracks that form in the mid-span of the beam.

In these beam specimens, all the length of flexural reinforcement is de-bonded within the shear span and a portion of mid-span. The bond of reinforcement and concrete in a portion between two point loads causes the flexural cracks to propagate in the mid-span of the beam and not to have shear crack, as long as it keeps the load carrying capacity of beams as much as the beams with full bond of reinforcement.

Table [5.1] shows the nominal values together with the experimentally obtained values of the load-carrying capacity and flexural capacity**.** It also includes the values of tensile stress of longitudinal reinforcement, and deflection of beams.

Specimen	Cross Section	N (kN)	M_f (kNm)	P_f (kN)	P_{exp} (kN)	M_{exp} (kNm)	Tensile Stress of Bars, $f_s\ (MPa)$	Deflection (mm)
1	Rectangular	0	79.3	202.1	195.8	76.9	553	36.1
2	Square	0	48.2	122.8	120.9	47.4	563	25.0
3	Rectangular	250	88.7	226.1	146.0	57.3	232	16.9
4	Rectangular	100	84.9	216.2	172.8	67.8	414	18.8
5	Rectangular	100	84.9	216.2	167.3	65.7	395	32.6
6	Square	50	49.9	127.1	82.0	32.2	315	24.1
7	Square	50	49.9	127.1	81.4	32.0	313	22.4
8	Square	100	51.1	130.3	90.5	35.5	325	21.7

Table 5.1: Calculated and experimental results of beam specimens.

By considering above table, and also Fig. [5.25] and [5.26], it can be seen that the beams with rectangular cross section has higher load carrying capacity than beams with square cross section. The value of a_v/d for rectangular cross sections is 2.9 and for square cross sections is 4.6, so by considering table [5.1], it can be concluded that the load carrying capacity in beams is inversely proportional to the value of a_v/d.

Placing stirrups is effective to face the tensile force which is formed in the interface between uncracked and cracked concrete, as it is shown in Fig. [4.2].

Applying axial load causes the beam to have lower load carrying capacity. For the beams with axial force, the below formula exists between the bending moment, compressive force and axial load:

$$M_{exp} = F_c\left(\frac{h}{2} - \frac{x}{2}\right) + (F_c - N)\left(\frac{h}{2} - d'\right) \Rightarrow M_{exp} = F_c\left(h - \frac{x}{2} - d'\right) - N(\frac{h}{2} - d')$$

The existence of axial load causes reduction of bending moment, and in the result, the reduction of load carrying capacity (P_{exp}). On the hand, based on the formula of:

$$F_s = F_c - N$$

Axial load also decreases the value of tensile force in the longitudinal reinforcement.

By comparing third and fourth beams and also seventh and eighth beams, it can be concluded that by decreasing the axial load from 250kN to 100kN caused the beam

to show higher capacity of tolerating the load and delayed the time of failure. Comparison of beam with axial loads of 100kN and 50kN, indicates that the beam with axial load of 100kN has higher load carrying capacity.

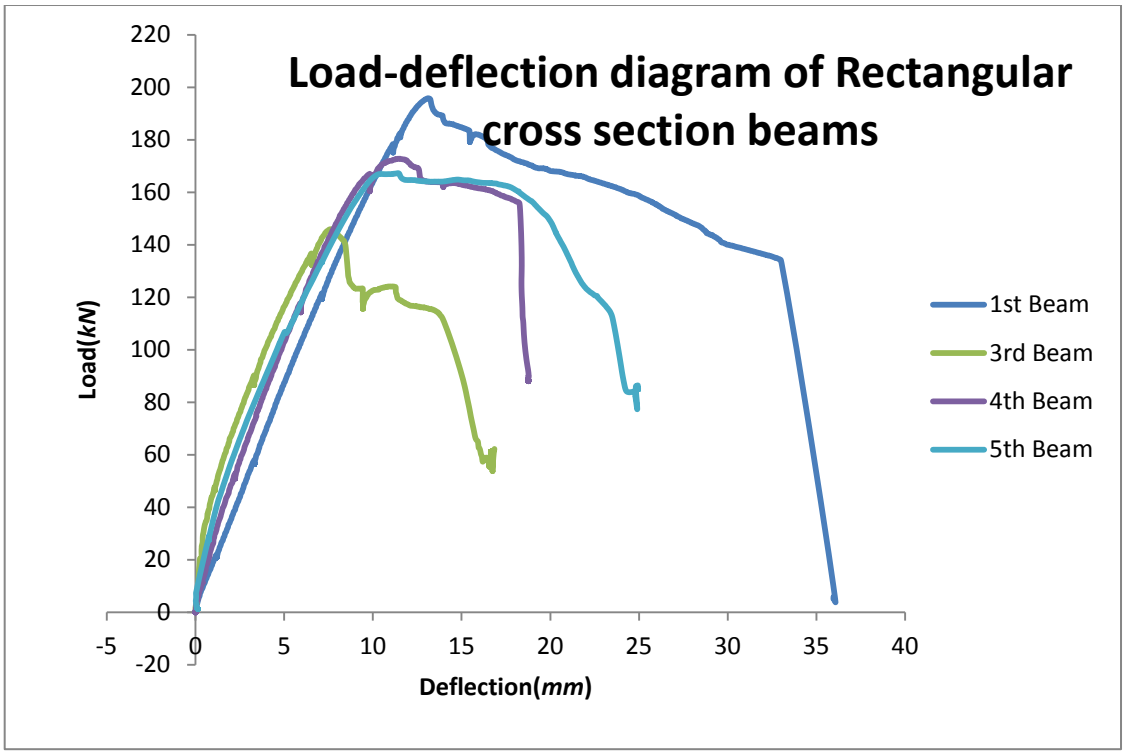

Figure 5.25: Load-deflection diagram of rectangular cross section beams.

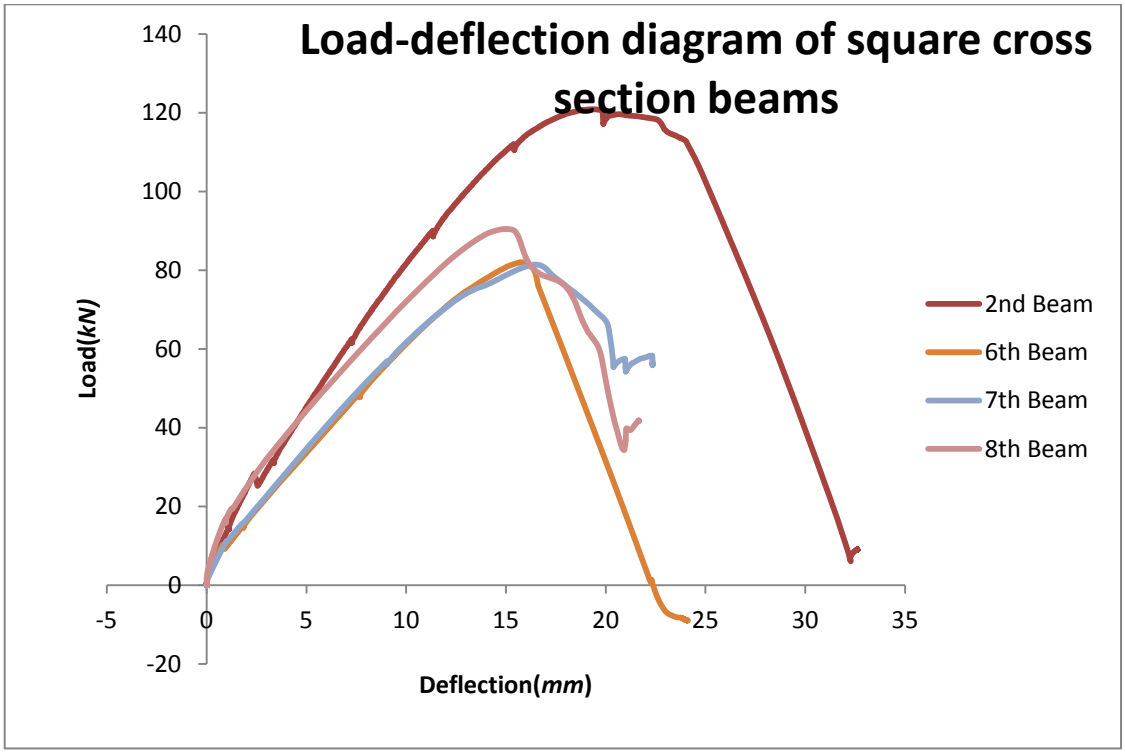

Figure 5.26: Load-deflection diagram of rectangular cross section beams.

The longitudinal reinforcement in all the beams including those with or without axial load, do not yield and all the beams fail because of concrete failure. In this case, the number and size of flexural reinforcement should be adjusted.

Chapter 6: Conclusions and Discussion

Exposure of flexural reinforcement in the middle of the beam causes the flexural cracks to propagate in the middle of the beam and not to have shear crack. Beams with rectangular cross section have more load carrying capacity than beams with square cross section. The stirrups are effective to face the tensile force in the shear span which is formed in the interface of uncracked and cracked concrete. Applying axial load reduces load carrying capacity and tensile force in longitudinal reinforcement. Comparison of beam with 250kN, 100kN and 50kN, indicates that the beam with axial load of 100kN has higher load carrying capacity. It is realized that the steel bars in all the beams did not yield and failure happened in concrete only. For further investigation, it is recommended to check the design of longitudinal reinforcements of the beam as it was designed based on full concrete-steel interaction. Thus, this new concept of the bond-prevented flexural failure may lead to savings of the amount of steel bars.

REFERENCES

1. American Concrete Institute, "*Building Code Requirements for Structural Concrete (ACI 318-02) and Commentary (ACI 318R-02)*". 2002.

2. Kotsovos M. D. and Pavlovic M. N. (1999), "Ultimate limit-state design of concrete structures: A new approach", Thomas Telford, *100pp*.

3. Kotsovos M. and Lefas, I. D. (1990), "Behaviour of Reinforced Concrete Beams Designed in Compliance with The Concept of Compressive Force Path", ACI Structural Journal, **87**, No. 2, 127-139.

4. Kani G. (1964), "The Riddle of Shear Failure and its Solution, ACI Journal, Proceedings", **61**, No. 4, 441-467.

5. Sharaf H. and Soudki K. (2002), "Strength Assessment of Reinforced concrete Beams with Debonded Reinforcement and Confinement with CFRP Wraps", 4th Structural Specialty Conference of the Canadian Society for Civil Engineering, Montreal, Quebec, Canada.

6. Kim W. and White R. N. (1999), "Shear-Critical Cracking in Slender Reinforced Concrete Beams", ACI Structural Journal, Title no. 96-S83.

7. Krefeld W.J., and Thurston C. W., "Contribution of Longitudinal Steel to Shear Resistance of Reinforced Concrete Beams," ACI JOURNAL, Proceedings V. **63**, No. 3, Mar. 1966, pp. 325-344.

8. Moody K. G., Viest I. M., Elstner R. C., and Hognestad E., "Shear Strength of Reinforced Concrete Beams-Parts 1 and 2," ACI JOURNAL, Proceedings V. **51**, No. 4, Dec. 1954, pp. 317-332, and No. 5, Jan. 1955, pp. 417-436.